THE JOURNAL OF PHYSICAL CHEMISTRY C

ARTICLE

pubs.acs.org/JPCC

Interaction of Water with FeO(111)/Pt(111): Environmental Effects and Influence of Oxygen

Franziska Ringleb,[†,#] Yuichi Fujimori,[†,#] Hui-Feng Wang,[†] Hiroko Ariga,[†] Esther Carrasco,[†] Martin Sterrer,[*,†] Hans-Joachim Freund,[†] Livia Giordano,[*,‡] Gianfranco Pacchioni,[‡] and Jacek Goniakowski[§,⊥]

[†]Department of Chemical Physics, Fritz-Haber-Institut der Max-Planck-Gesellschaft, Faradayweg 4-6, 14195 Berlin, Germany

[‡]Dipartimento di Scienza dei Materiali, Università di Milano-Bicocca, via Cozzi, 53, 20125 Milano, Italy

[§]CNRS, Institut des Nanosciences de Paris, UMR 7588, 4 Place Jussieu, 75252 Paris cedex 05, France

[⊥]UPMC Université Paris 06, INSP, UMR 7588, 4 Place Jussieu, 75252 Paris cedex 05, France

Supporting Information

ABSTRACT: The structural and chemical properties of a monolayer FeO(111)/Pt(111) exposed to air, liquid water, and controlled atmospheres of water vapor and water vapor/oxygen mixtures have been studied by a combination of infrared spectroscopy, X-ray photoelectron spectroscopy, and scanning tunneling microscopy experiments together with density functional calculations using ab initio thermodynamics. The FeO(111)/Pt(111) film is inert toward pure water vapor up to mbar pressure. Coadsorption of oxygen and water, however, transforms the film into a hydroxyl terminated trilayer with a (Pt−)O−Fe−OH structural motif. The trilayer film forms spontaneously upon contact of FeO(111)/Pt(111) with air and preserves long-range order even in liquid water. The calculated phase diagram in the relevant range of oxygen and water chemical potentials is in agreement with the experimental results and shows that the oxygen chemical potential is the main driving force for the formation of the trilayer film. Results for Au nucleation on and CO oxidation over the FeO(OH) film are presented and compared to previous studies on nonhydroxylated films.

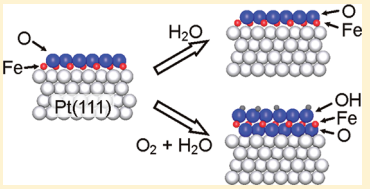

1. INTRODUCTION

The dissociative chemisorption of water on solid surfaces is the subject of major interest in surface science because of the strong impact of hydroxyl groups on the surface properties, in particular, the reactivity of solid surfaces. Besides the enormous importance in electrochemical and photoelectrochemical water splitting, where water dissociation is driven by external parameters, the fundamental understanding of water interaction with well-defined solid surfaces is still the subject of active research. While in some cases there is controversy about the mode of adsorption, dissociative or molecular, it is generally accepted that surface defects, in particular on oxide surfaces, give rise to spontaneous water dissociation. In addition, water dissociation was shown to be enhanced on otherwise unreactive surfaces by promoters such as oxygen or alkali adatoms.[1,2]

Polar oxide surfaces are intrinsically reactive toward water because surface hydroxyls provide compensating charges necessary to remove polarity.[3,4] Similarly, in polar oxide films grown on metal substrates, while the compensating charge density at the metal−oxide interface is readily provided by the metal,[5] the free film surface needs to be compensated by conventional mechanisms, for example, surface hydroxylation. Conversely, the thinnest oxide films (monolayers) are intrinsically nonpolar thus reducing their activity toward water. However, the electron exchange with the metal substrate[6,7] and the substrate-induced rumpling (polarization)[4,8] may considerably influence their properties.[9,10]

In this work, we show that one monolayer (ML) FeO(111) grown on Pt(111) is relatively inert toward water. Conversely, a polar FeO_2/Pt(111) film, which is obtained at higher oxygen partial pressure, readily hydrogenates in the presence of water and maintains long-range order in air and even in liquid water.

FeO(111) films grown on Pt(111) have been the subject of many ultrahigh vacuum investigations in the past.[11,12] The most peculiar feature of the FeO(111)/Pt(111) system is the periodic variation of the interface structure imposed by the lattice mismatch between FeO(111) and Pt(111), which leads to the formation of a Moiré superlattice with three high-symmetry domains with Fe either in on-top, hexagonal close-packed (hcp), or face-centered cubic (fcc) stacking with respect to the interfacial Pt atoms. Several investigations, using scanning tunneling microscopy, focused on the domain structure as well as on the adsorption of molecules and metals in domains within the unit cell.[13−19] The perfect, oxygen-terminated FeO(111) is chemically inert under ultrahigh vacuum conditions. Notably, only atomic hydrogen has been shown to significantly interact with the surface leading to reduction of the film.[20−22] Molecular water only weakly interacts with the FeO(111)/Pt(111) surface.[23−25] However, it readily dissociates even under ultrahigh vacuum (UHV) conditions at FeO(111) step edges exposed in submonolayer films.[26] Similarly, the dissociation

Received: August 1, 2011
Revised: August 23, 2011
Published: August 24, 2011

ACS Publications © 2011 American Chemical Society

of aliphatic alcohols has been shown to preferentially proceed at step edges.[27]

Aiming at elucidating the catalytic activity of FeO(111)/Pt(111) in CO oxidation, its properties have recently been investigated also under elevated pressure conditions, that is, mbar atmospheres of O_2 and CO. Most interestingly, in CO-rich atmosphere, the film undergoes dewetting with complete loss of structural order, whereas a new ordered phase with apparent 2:1/O:Fe stoichiometry forms in oxygen-rich environment.[28] Density functional calculations revealed that the structural transition from a (Pt−)Fe−O bilayer to a (Pt−)O−Fe−O trilayer occurs preferentially within the hcp domains and that it is accompanied by an electron transfer toward the oxide film and a change of oxidation state of cations from Fe^{2+} to Fe^{3+}.[29,30] The enhanced CO oxidation activity of the trilayer phase has been demonstrated for both the flat FeO(111)/Pt(111) and the FeO(111) overlayers that grow on Fe_3O_4-supported Pt particles after thermal treatment above 850 K.[28,31]

The catalytic results reported so far have been obtained with samples that were transferred under clean conditions from UHV environment into dedicated high-pressure cells. In any realistic environment, for example, air, the surface will, however, also be exposed to traces of water. A crucial parameter for catalytic applications is, therefore, if the catalytically active phase, that is, the O−Fe−O trilayer, is also stable under more realistic conditions. In this paper, we present a combined experimental and computational investigation on the interaction of FeO(111)/Pt(111) with air and water. Scanning tunneling microcopy (STM), X-ray photoelectron spectroscopy (XPS), and infrared reflection absorption spectroscopy (IRAS) were used to study the structure and chemical composition of a UHV-prepared FeO(111) surface in/after contact with air and liquid water as well as after controlled exposure to high pressures of water vapor and water vapor/oxygen mixtures. The interaction of water with FeO(111)/Pt(111) was investigated, and the FeO_xH_y/Pt phase diagram was determined in the relevant range of oxygen and water chemical potentials using ab initio thermodynamics. Our results show that the FeO film is relatively inert toward water vapor in the mbar range. However, it readily transforms into a trilayer with terminating OH groups in air and water vapor/oxygen mixtures. We show that the long-range order of the film is preserved even in liquid water and that the modified FeO(OH) trilayer exhibits catalytic activity in CO oxidation that is as similarly high as the unmodified one reported previously.

2. EXPERIMENTAL AND COMPUTATIONAL PROCEDURES

The experiments were performed in two separate UHV chambers equipped with standard tools for single crystal cleaning and thin film preparation. For spectroscopic studies, the sample was directly fixed by tantalum wires to molybdenum rods on a manipulator, which allowed for direct heating of the sample and cooling to 90 K using liquid nitrogen. The UHV apparatus used for spectroscopic studies is equipped with an X-ray gun and a hemispherical analyzer for XPS investigations as well as a low-energy electron diffraction (LEED) apparatus and a mass spectrometer. In addition, a small UHV/high-pressure cell connected to the UHV chamber, which is equipped with CaF_2 windows for optical access to infrared radiation, allows for adsorption experiments from UHV up to the mbar range. For STM studies in ambient air and liquid water, the sample was mounted on an Omicron sample holder with an attached filament for electron beam heating. The sample was transferred from the UHV chamber via a load lock to the STM. In both chambers, the temperature of the sample was measured with a chromel/alumel thermocouple.

The Pt(111) single crystal was cleaned by room-temperature sputtering (Ar^+) followed by a short anneal to 1200 K in UHV, subsequent oxidation at 600 K in 1×10^{-6} mbar O_2, and a final anneal to 1200 K in vacuum. The surface quality and cleanness of the Pt(111) substrate was checked with LEED and XPS. FeO(111) thin films were grown following procedures described in the literature.[12] First, 1 ML Fe was deposited on Pt(111) in UHV at room temperature. The sample was then heated in a background pressure of 1×10^{-6} mbar O_2 to 970 K (2 min), was cooled in oxygen to 500 K, and finally was cooled to room temperature in UHV. The final FeO film was characterized by LEED showing the typical Moiré pattern of the FeO(111)/Pt(111) system, XPS, and temperature-programmed desorption experiments of adsorbed CO to confirm that the Pt(111) is fully covered by FeO.

Water adsorption and water/oxygen coadsorption were carried out at room temperature in the UHV/high-pressure cell. The pressure was measured with a Baratron gauge (range 10^{-2}−1000 mbar) directly attached to the cell. Deionized water was cleaned by repeated freeze−pump−thaw cycles prior to inlet into the cell.

Infrared spectra were acquired with a Bruker IFS66v spectrometer and an external mercury cadmium telluride (MCT) detector either in the standard reflection absorption (IRAS) mode or with the polarization modulation (PM-IRAS) technique using a photoelastic modulator (Hinds Instruments). Typically, 1000 scans were accumulated for one spectrum and the resolution was set to 4 cm^{-1}. XPS spectra of the O 1s and Fe 2p regions were acquired using a dual anode X-ray source (Specs XR50) in combination with a hemispherical analyzer (Specs Phoibos150). All spectra reported here are referenced to the Fermi energy of Pt(111) and were taken at an electron takeoff angle of 60° with analyzer pass energy set to 20 eV. For quantitative evaluation, the O 1s spectra were fit using two components, one for the oxide film and one for hydroxyls. Linear backgrounds were chosen for this spectral region.

For STM experiments in ambient air and in liquid water, we used a Wandelt-type electrochemical STM[32] with a modified liquid cell that fits our sample holder. For STM measurements in liquid H_2O, insulated Pt/Ir tips were used.

The computational setup is similar to the one used in our earlier studies on the FeO/Pt(111) system.[9,17,30] We use the density functional theory (DFT) approach in the DFT + U variant to correct the inherent limitations of the method in describing late transition metal oxides with localized states. We adopt the approach of Dudarev et al.,[33] as implemented in the VASP code,[34,35] with $U_{Fe} - J_{Fe} = 3$ eV. The calculations have been performed within the generalized gradient approximation using the Perdew−Wang 91 (PW91) functional,[36] a plane wave basis set with kinetic energy cutoff of 400 eV, and the projector augmented wave method.[37,38]

In the present study, we use the (2×2)-FeO(111) on (2×2)-Pt(111) pseudomorphic interface model, which has already been employed to construct the FeO(111) film phase diagram as a function of the oxygen chemical potential.[30] We have restricted our analysis to the Fe-hcp region, where the FeO_2 trilayer is preferentially formed. Within this model, the interface oxygens are on-top of the surface Pt atoms and the in-plane position of

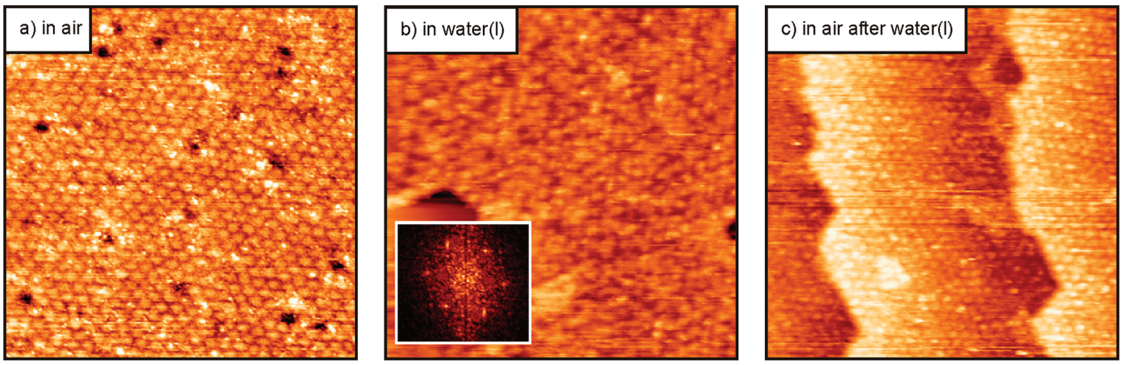

Figure 1. STM images (60 nm × 60 nm) of FeO(111)/Pt(111) prepared in UHV and imaged in (a) air, (b) deionized water, and (c) air again after removing water . The inset in b shows an FFT of the image revealing the hexagonal array of protrusions on the surface in liquid water.

two of them is kept fixed to maintain the interface registry. The lattices are aligned and the Pt(111) substrate is expanded in order to match the oxide in-plane lattice parameter (a = 3.10 Å). The magnetic ordering in the considered iron oxides corresponds to a row-wise antiferromagnetic structure, RW-AF-(2 × 1), used previously for FeO(111)/Pt(111). The Pt(111) substrate is represented by five atomic layers, and the oxide film is adsorbed on one side of the metal slab. The slabs are separated by at least 10 Å of vacuum, and the dipole correction is applied in order to eliminate the residual dipoles in the direction perpendicular to the surface. All the other coordinates of the oxide films and the vertical coordinates of Pt atoms are allowed to relax until the residual forces are smaller than 0.01 eV/Å. The Brillouin zone is sampled on a (5 × 5 × 1) Monkhorst−Pack grid.

We analyze the interaction of the iron oxide film with a water atmosphere or water/oxygen mixtures by considering $FeO_{1+x}(OH)_y$ phases ranging from dry FeO to the fully hydroxylated FeO(OH) oxide film. Different stages of oxidation and hydroxylation are described by imposing the chemical equilibrium between the oxide film and the reservoirs of O_2 and H_2O molecules in the gas phase, at a given partial pressure and temperature, characterized by the chemical potentials μ_O and μ_{H_2O}, respectively. The variation of Gibbs free energy with respect to a clean FeO/Pt(111) film can be written as

$$\Delta G = G(FeO_{1+x}(OH)_y/Pt) - G(FeO/Pt) - (y/2)\mu_{H_2O} - (y/2 + x)\mu_O$$

Following the usual procedure in ab initio thermodynamics,[39] ΔG is approximated by the difference of the corresponding 0 K total energies $E(FeO_{1+x}(OH)_y/Pt) - E(FeO/Pt)$ and of the chemical potentials of gas phases. We have referred the chemical potentials to the total energies of the corresponding isolated molecules, namely, $\mu_O(0\ K, p) = {}^1/_2E(O_2) = 0$ and $\mu_{H_2O}(0\ K, p) = E(H_2O) = 0$.

3. RESULTS

3.1. Environmental Effects: Interaction of FeO(111) with Air and Liquid Water. In Figure 1, we present STM images of FeO(111)/Pt(111) taken in air (a), in liquid water (b), and again in air after removing liquid water and subsequent drying (c). The image taken in air (Figure 1a) shows a periodic structure that appears similar to the Moiré superstructure observed for FeO-(111)/Pt(111) in UHV.[40] Under the present experimental conditions (high oxygen partial pressure), however, the FeO film more likely transforms into a FeO_{2-x} film as previously

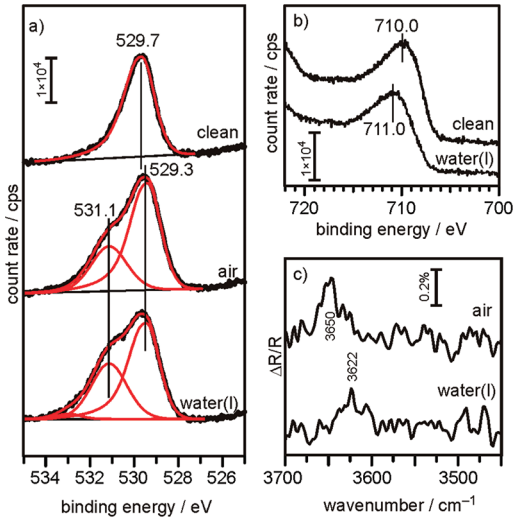

Figure 2. XPS and PM-IRAS spectra from clean FeO(111)/Pt(111) and after contact with air and liquid water. (a) XPS O 1s region, (b) XPS Fe 2p region, (c) PM-IRAS OH region.

observed after high-pressure oxygen treatment of FeO(111).[28,29] We will show below XPS spectra that will shed more light on the chemical composition of the film in air. The in-situ STM image taken of the FeO(111) surface in contact with liquid water (Figure 1b) reveals more structural disorder as compared to Figure 1a. The fast Fourier transform (FFT) taken from this image (see inset in Figure 1b), however, provides evidence for hexagonal symmetry of the structures observed in Figure 1b. Most notably, after removing liquid water, the film is similarly as well ordered as before water treatment (Figure 1c).

The chemical state and the surface termination of the FeO-(111) films after various treatments were determined by XPS and infrared spectroscopy. Figure 2a shows the O 1s XP spectrum of the clean FeO(111) film (top) and after exposure to air (middle) and liquid water (bottom). The clean film exhibits a single O 1s component at 529.7 eV.[12,41] Upon exposure to air, this component shifts to lower binding energies (529.3 eV), and its intensity slightly increases compared to the clean sample. The shoulder appearing on the high-binding energy side of this peak can be fitted with a second component exhibiting a binding energy of 531.1 eV consistent with the O 1s of hydroxyls.[42,43] After liquid water treatment, the O 1s region only slightly changed as compared to air exposure with more intensity in the hydroxyl

dx.doi.org/10.1021/jp207332n |J. Phys. Chem. C 2011, 115, 19328–19335

Table 1. Amount of OH Produced by Exposure of FeO(111)/Pt(111) to Air and Liquid Water (Figure 2a)

	O−Fe−**OH**
clean FeO(111)	0
air	0.48
water	0.63

peak and slightly less in the oxide peak (Figure 2a). Changes upon exposure to air and water are also observed in the Fe 2p region with a shift of the peak from 710.0 eV for exclusively Fe^{2+} in the clean FeO(111) film to 711.0 eV after exposure to water indicating oxidation of Fe^{2+} to Fe^{3+} (Figure 2b).[42,43] Finally, PM-IRAS spectra measured after air and liquid water exposure of FeO(111) indicate the formation of surface hydroxyl groups exhibiting stretching frequencies in the range 3620−3650 cm^{-1} (Figure 2c).

The STM images of Figure 1 provide ample evidence for the stability of the monolayer iron oxide film on Pt(111) in the various environments with no sign of dewetting even in liquid water. Spectroscopic characterization, however, gives clear indication of chemical modification of the film with significant enrichment with oxygen, oxidation of Fe^{2+} to Fe^{3+}, and hydroxyl termination. On the basis of integration of the O 1s peak components of the clean and modified films (Figure 1b), a hydroxyl coverage of, respectively, 0.48 ML in air and 0.63 ML after water treatment (Table 1) is estimated (where 1 ML is defined with respect to the full oxygen monolayer in the clean FeO(111) film). The results are compatible with the transformation of the (Pt−)Fe−O bilayer film into a trilayer film under the action of the high oxygen chemical potential.[29] However, unlike an oxygen termination, (Pt−)O−Fe−O, such as observed previously after mbar O_2 treatment of FeO(111) at 450 K, in the present case the surface is terminated by hydroxyl groups calling for a structure similar to (Pt−)O−Fe−OH. This observation consequently requires molecular water to be dissociatively adsorbed on the surface. To check the reactivity of the FeO(111) film toward environmental gases in the relevant range of pressures, we, therefore, investigated its interaction with water vapor and water/oxygen mixtures under controlled conditions in a high-pressure cell.

3.2. Interaction with Water Vapor and Water/Oxygen Coadsorption. Figure 3a summarizes the XPS results obtained for dosing water at increasing water vapor pressures from 1 × 10^{-2} mbar up to 10 mbar at room temperature to a clean FeO(111) film. The clean FeO(111) film exhibits an O 1s peak at a binding energy of 529.6 eV (Figure 3a). No significant change of the O 1s peak is observed after dosing water at 1 × 10^{-2} and 1 mbar H_2O. Only after interaction of FeO(111) with 10 mbar H_2O can a small shoulder on the high-binding energy side of the main O 1s peak be observed. The peak at 531.4 eV is consistent with the O 1s binding energy of hydroxyl groups on FeO(111), although this peak is shifted by about 0.3 eV to higher binding energy compared to the sample exposed to air (Figure 2a). In addition, no shift of the main O 1s peak is observed. The corresponding IRAS spectrum in Figure 3b reveals the formation of OH groups exhibiting a stretching frequency in the range ν(OH) = 3560−3590 cm^{-1}, which is significantly lower than the IR band observed in Figure 2c.

The data presented in Figure 3a and b is consistent with the inertness of FeO(111) toward water vapor reported in previous UHV studies. The tiny amount of hydroxylation observed after 10 mbar H_2O might be related to a defect-mediated water

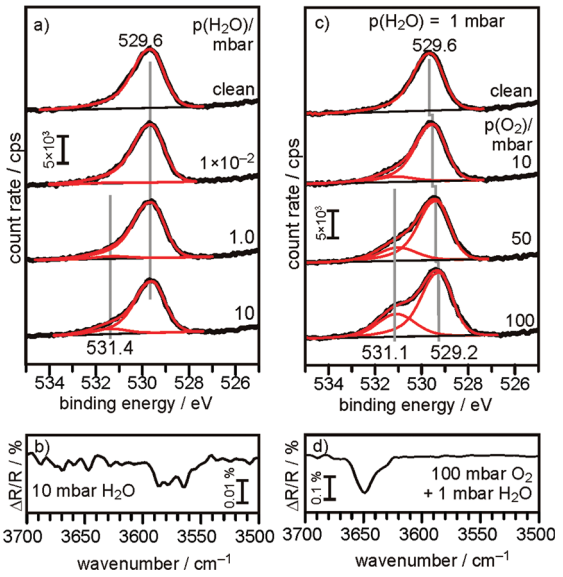

Figure 3. (a) O 1s XPS spectra of clean FeO(111)/Pt(111) and after interaction with water vapor for 3 min at room temperature at the indicated pressure. (b) IRAS spectrum obtained after interaction of 10 mbar H_2O with FeO(111). (c) O 1s XPS spectra of clean FeO(111)/Pt(111) and after H_2O/O_2 coadsorption for 3 min at room temperature. The H_2O pressure was fixed at 1 mbar. (d) IRAS spectrum obtained after coadsorption of 1 mbar H_2O and 100 mbar O_2.

Table 2. Amount of OH Produced on FeO(111)/Pt(111) in the H_2O/O_2 Coadsorption Experiment (Figure 3c)

	O−Fe−**OH**
clean FeO(111)	0
10 mbar O_2	0.10
50 mbar O_2	0.26
100 mbar O_2	0.45

dissociation with the formation of (Pt−)Fe−OH species. In fact, exposure of FeO(111) to atomic hydrogen leads to strong hydroxylation and the production of hydroxyl groups at the expense of lattice oxygen.[20−22] These hydroxyl groups exhibit a similar stretching frequency of ν(OH) = 3580 cm^{-1} as observed in Figure 3b and can be assigned to (Pt−)Fe−OH species in disordered surface structures (see Supporting Information, Figure S1).

For the water/oxygen coadsorption experiments shown in Figure 3c and d, the water partial pressure was fixed at 1 mbar and the oxygen partial pressure was varied between 10 and 100 mbar. With increasing oxygen pressure, enhanced formation of hydroxyl groups with a characteristic binding energy of 531.1 eV is detected. Table 2 lists the amount of hydroxyls (in monolayers with respect to the close-packed oxygen layer of the clean FeO film) formed in the individual experiments. Increasing the oxygen pressure above 100 mbar did not enhance the formation of hydroxyls. Comparison with the quantitative estimate of hydroxyl coverage after exposure to air (Figure 2a, Table 1) reveals a similar degree of hydroxylation for the sample exposed to 100 mbar O_2 and 1 mbar H_2O. In addition, the progressive shift of the main O 1s peak to lower binding energy as the oxygen partial pressure is increased resembles the result of the experiment shown in Figure 2a. Finally, the stretching frequency of the

Table 3. Adsorption Energies (in eV/H_2O) of Water Adsorbed in Molecular (E_m) and Dissociative (E_d) Mode on the FeO(111)/Pt(111) Substrate Calculated for 0.25, 0.50, and 1.00 ML Water Coverage[a]

	θ = 0.25 ML	θ = 0.50 ML	θ = 1.00 ML
E_m(eV/H_2O)	0.07	0.46	0.48
E_d(eV/H_2O)	0.18	0.30	0.27

[a] A positive value of E_m or E_d indicates a bound state.

OH groups formed in the coadsorption experiment is at ν(OH) = 3650 cm^{-1}, which is similar to that observed after exposure to air (Figure 2c).

By exposure of FeO(111) to mixtures of O_2 and H_2O, we could closely reproduce the chemical changes of the FeO(111) film observed after air treatment. The results show that the presence of oxygen is necessary to achieve significant hydroxylation of the film. As a consequence, and similar to results obtained for pure oxygen, these results suggest that the FeO film transforms into a trilayer film, however, with terminating OH groups and a (Pt−)O−Fe−OH structural motif. Support for this transformation is provided by the oxygen enrichment and by the observed shift of the main O 1s XPS peak to lower binding energies. The latter can be explained by enhanced screening of the core holes created in oxygen layers directly adjacent to the Pt substrate in the trilayer film as compared to the oxygen layer on-top of iron in the clean FeO(111) film. Interestingly, the resulting O−Fe−OH structural motif is also the building block of the naturally occurring mineral goethite (FeOOH), and the observed stretching frequency of 3650 cm^{-1} (Figure 2c, 3d) is close to the stretching frequency of OH groups on bulk goethite (3660 cm^{-1}).[44]

3.3. Ab-Initio Investigation of Water Adsorption on FeO(111). To address the nature of interaction between water and the supported FeO(111) film, water adsorption at different water coverage has been investigated by DFT calculations. The reported results are obtained for the Fe-hcp region of the Moiré pattern.

Table 3 summarizes the calculated adsorption energies for water adsorbed in molecular (E_m) and dissociative (E_d) modes as a function of the coverage.

A single water molecule (0.25 ML) binds only weakly to the FeO/Pt(111) substrate and shows a preference for the dissociative adsorption mode. Upon dissociation, the OH group binds on-top of a Fe atom, which relaxes outward, reversing locally the film rumpling. Because of this structural distortion, the remaining hydrogen adsorbs at surface oxygen second neighbor, so that the two OH groups formed upon dissociation are not linked by a hydrogen bond.

The presence of additional water molecules stabilizes both molecular and dissociative water adsorption modes. In the case of molecular adsorption, the stabilization is driven mainly by the interaction between the coadsorbed molecules with formation of hydrogen bonds. The increase of adsorption energy as function of coverage indicates a tendency of adsorbed molecules to cluster resulting in regions of bare and fully hydrated substrate. Since the interaction between the coadsorbates is of the same order of that with the substrate, water clusters are expected to adopt a three-dimensional form.

In the case of dissociative adsorption, the stabilizing interaction between water fragments is weaker. However, E_d reported in Table 3 refers to the final state in which H and OH issued from water dissociation form a mixed surface phase. Neglecting possible kinetic hindering, an alternative final state consists of separated OH-rich FeO$(OH)_y$ and H-rich $FeOH_y$ regions. Since, according to our calculations, the effective interaction between coadsorbed OH groups is attractive and that between coadsorbed H is repulsive, we use, respectively, FeO$(OH)_{1.00}$ and $FeOH_{0.25}$ phases to estimate the corresponding adsorption energy. We find that water dissociation followed by phase separation is exothermic by 0.45 eV/H_2O. It is favored over dissociation into a mixed phase but is somewhat less advantageous than formation of clusters of molecularly adsorbed water.

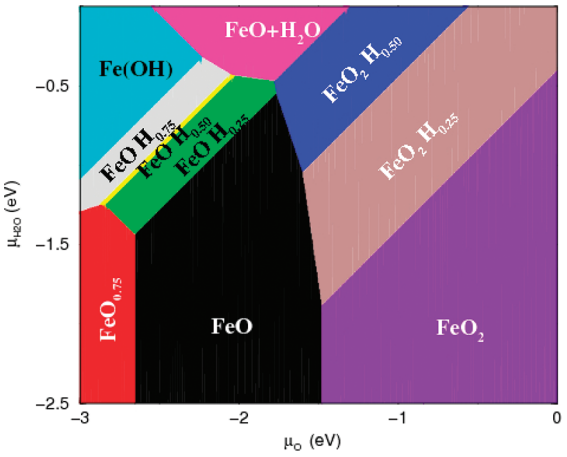

Figure 4. Phase diagram of the most stable structures of the FeO/Pt(111) film in equilibrium with H_2O and O_2 as a function of oxygen μ_O and water μ_{H_2O} chemical potentials (eV).

In summary, water molecules interact only weakly with the Pt-supported FeO(111) film. Under UHV conditions and at low temperatures, we expect water to form molecular water clusters weakly bound to the support. Calculated adsorption energies are smaller than 0.5 eV/molecule suggesting that water will desorb below room temperature. This result is in agreement with previous UHV studies addressing water adsorption on FeO(111)/Pt(111)[24,25] and with our own IR studies reported in the Supporting Information (Figure S2).

3.4. Thermodynamics of FeO(111)/Pt(111) with Water/Oxygen Coadsorption. To address the thermodynamic stability of the FeO(111) film in the presence of water and oxygen, we have constructed the stability diagram of the Pt-supported ordered $FeO_{1+x}(OH)_y$ phases as a function of oxygen and water chemical potentials, Figure 4. While several alternative configurations for each value of (x, y) have been considered and optimized, only the most stable ones are represented in Figure 4.

In H_2O-poor conditions ($\mu_{H_2O} < -2$ eV), we recover the oxidation characteristics of the dry FeO(111)/Pt(111) system described in our previous study.[30] In particular, in extremely oxygen-poor conditions ($\mu_O < -2.8$ eV), oxygen vacancies (red in Figure 4) are formed in the FeO(111) film. The stoichiometric FeO film (black) is stable for -2.8 eV $< \mu_O < -1.5$ eV, and the FeO_2 trilayer (purple) appears at higher values of the oxygen chemical potentials ($\mu_O > -1.5$ eV).

For intermediate values of water chemical potential (-2 eV $< \mu_{H_2O} < -1$ eV), a progressive hydrogenation of the oxide film takes place. At low μ_O, as the water chemical potential increases, we find $FeOH_y$ films with y = 0.25 (green in Figure 4), y = 0.50 (yellow), y = 0.75 (gray), and y = 1.0 ML (light blue) surface hydrogens. Similarly, at high μ_O, we find FeO_2H_y trilayers with y = 0.25 (brown) and y = 0.50 (blue). At intermediate values of μ_O,

the clean FeO phase (black) is stable, but its stability domain shrinks progressively with the increasing water chemical potential. This phase disappears eventually for $\mu_{H_2O} > -0.6$ eV. We notice that hydrogenation of FeO_2 starts at lower μ_{H_2O} compared to that of FeO. This is coherent with the experimental results showing easy formation of a hydrogenated FeO_2 film, Table 2, and with the expected higher activity of the polar $FeO_2(111)$ trilayer. However, while hydrogen is always more strongly bound to the trilayer, the hydrogenation does not modify substantially the trilayer electronic structure and, in particular, does not alter the oxidation state of the cations. This is consistent with the observed good stability of dry $FeO_2(111)$ trilayer and suggests that the energetics of polarity compensation plays a secondary role in the transformation of FeO into FeO_2 under water vapor.

Finally, in extremely H_2O-rich conditions ($\mu_{H_2O} > -0.5$ eV), FeO with a 1 ML of molecularly adsorbed water (pink in Figure 4) becomes progressively the most stable structure in the whole range of considered μ_O. As a consequence, in agreement with the results on water adsorption characteristics, section 3.3, molecularly adsorbed water is thermodynamically most stable at the highest water pressures.

As shown by the experiment, the formation of the $FeO_2(111)$ trilayer is driven mainly by the oxygen pressure, and the stabilizing effect of water is relatively small. Indeed, the value of μ_O at which the relative stability of both clean and hydrogenated FeO(111) and $FeO_2(111)$ films is inverted depends only slightly on the water chemical potential μ_{H_2O}: it decreases by −0.25 eV only between water-poor ($\mu_{H_2O} < -2.0$ eV) and water-rich ($\mu_{H_2O} \approx -0.6$ eV) limits. This weak effect of μ_{H_2O} can be traced back to the relatively strong bonding of oxygen in the H_2O molecules: $^1/_2E(O_2) > E(H_2O) - E(H_2)$, where E is the computed 0 K total energy. As a consequence, while film oxidation under molecular oxygen FeO + $^1/_2O_2 \rightarrow FeO_2$ is exothermic by about 1.5 eV/Fe, the oxidation with water molecules FeO + $H_2O \rightarrow FeO_2 + H_2$ is endothermic by 1.2 eV/Fe, and similarly the hydrogenation FeO + $H_2O \rightarrow$ FeO(OH) + $^1/_2H_2$ is endothermic by 0.4 eV/Fe.

The above results show that the relative thermodynamic stability of FeO and FeO_2 films is mainly driven by the oxygen chemical potential and that formation of the (hydrogenated) FeO_2 trilayer is only slightly easier in the presence of water. As a consequence, in agreement with the experimental findings, at low oxygen pressure ($\mu_O < -1.8$ eV), neither dry nor (partially) hydrogenated FeO_2 trilayer can be stabilized. Conversely, an increase of μ_O beyond −1.5 eV results in stabilization of dry or (partially) hydrogenated FeO_2 trilayer.

3.5. Properties of the FeO(OH) Surface. To probe the properties of the FeO(OH) surface, we compared the Au nucleation behavior on this surface with Au on clean FeO(111) and tested its activity in CO oxidation at elevated pressure conditions.

(a). Gold Nucleation. Gold nucleation on FeO(111)/Pt(111) has been previously studied with STM as well as with IR spectroscopy and temperature-programmed desorption of adsorbed CO.[45,46] The interaction of Au with FeO(111) was found to be rather weak, and facile agglomeration into large particles occurs at elevated temperature. In this study, we compared the nucleation behavior of Au on clean FeO(111) and FeO(OH). Binding energy shifts observed in XPS together with observations of changes in the OH stretching region by IRAS have been shown to be valuable properties to describe the oxidation state and the particle size differences for gold nucleated on hydroxylated and nonhydroxylated substrates[47] and have also been used in the present study.

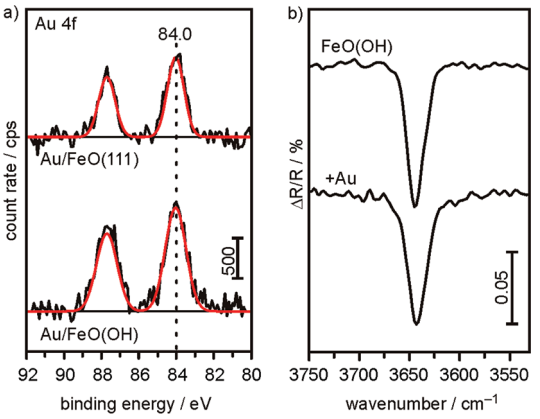

Figure 5. (a) Au 4f XPS spectra of 0.1 Å Au deposited at room temperature on FeO(111) (top) and FeO(OH) (bottom). (b) IRAS spectra of the OH region of FeO(OH) before (top) and after (bottom) deposition of 0.1 Å Au.

Figure 5a shows the Au 4f XP spectra of 0.1 Å Au deposited at room temperature on clean FeO(111) and FeO(OH). In both spectra, the Au $4f_{7/2}$ component is found at a binding energy of 84.0 eV, which is the same as for bulk gold and which is compatible with neutral Au atoms in moderately large particles. The absence of any binding energy shift compared to bulk gold in both samples indicates similar nucleation properties with neither different Au particle size nor oxidized Au species on the FeO(OH) sample. This conclusion is corroborated by the observation that the OH band at 3645 cm^{-1} observed on the FeO(OH) surface is not subjected to any change after gold deposition indicating only weak, if any, chemical interaction between Au and OH.

Recently, it has been shown that the interaction of Au with surface hydroxyls strongly depends on the nature of the hydroxyl groups leading either to enhanced agglomeration as, for example, observed on $TiO_2(110)$ with bridging hydroxyls[48] or to enhanced stability of small clusters and formation of oxidized gold species as observed on hydroxylated MgO(001).[47,49] In the present case, the reason for the rather weak interaction between Au and the surface may be found in the fact that the FeO(OH) surface is terminated by a high density of chemically similar OH groups. This results in a homogeneous and flat surface potential that facilitates diffusion and agglomeration of Au.

(b). CO Oxidation. Previous reports demonstrated the high reactivity of the FeO(111)/Pt(111) film in CO oxidation under oxygen-rich conditions.[28] The catalytically active phase has been identified to be a (Pt−)O−Fe−O trilayer that forms at high chemical potentials of oxygen.[29] To check whether the hydroxylated trilayer is similarly active in CO oxidation, we tested our films in the infrared high pressure cell under similar conditions as in ref 28 (10 mbar CO, 50 mbar O_2, T = 450 K).

Figure 6a shows the evolution of the gas-phase infrared spectra of CO and CO_2 during the catalytic reaction. Spectra were recorded in intervals of 10 min. From Figure 6b, which presents the integrated intensities of the gas-phase IR signals as a function of reaction time, a rapid consumption of CO, which follows an almost linear trend and which is complete after approximately 60 min, is evident. (For comparison, the dotted lines in Figure 6b are obtained for CO oxidation under similar conditions on the clean Pt(111) surface.) The calculated CO_2 formation rate is 4×10^{16} molecules $\cdot cm^{-2} \cdot s^{-1}$. The high CO oxidation activity resembles

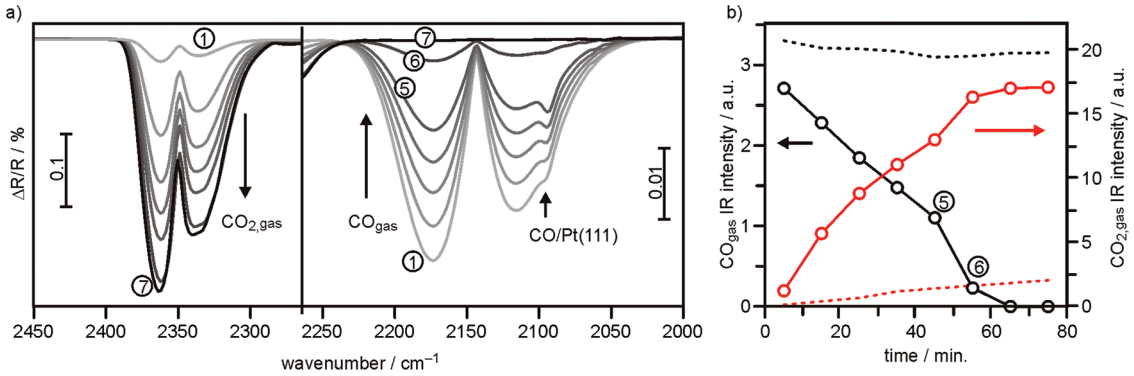

Figure 6. (a) Infrared spectra of the CO_2 (left) and CO (right) gas-phase spectral regions recorded during CO oxidation (10 mbar CO, 50 mbar O_2, 450 K) over FeO(OH). The spectra were recorded in intervals of 10 min. (b) Integrated intensities of the CO and CO_2 gas-phase IR signals as a function of reaction time (solid lines). For comparison, the CO consumption and the CO_2 production during CO oxidation on Pt(111) under similar reaction conditions are plotted as dotted lines.

the result of previous studies with the nonhydroxylated FeO_2 film[28] showing that the hydroxylated film is similarly active in CO oxidation. The structural (LEED) and chemical (O 1s and Fe 2p XPS and OH-IR) properties of the (Pt−)O−Fe−OH film determined after reaction were the same as that of the initial surface before reaction. Close inspection of the CO region in Figure 6a reveals, however, an additional infrared absorption at 2090 cm^{-1}, which can be assigned to CO adsorbed at on-top sites of the Pt(111) surface. Most interestingly, this spectral contribution disappeared almost completely in spectrum 6, when nearly all the CO was consumed (Figure 6a). At the same time, a clear increase in CO consumption is observed (Figure 6b). The appearance of the CO/Pt(111) IR signal at the beginning of the reaction can be explained by partial dewetting of the film induced by the high initial CO partial pressure in the reaction cell, which leads to open Pt(111) patches on the surface. As the reaction proceeds, the CO partial pressure continuously decreases and, after around 50 min, it reaches a critical lower value at which the completely oxidized trilayer film is thermodynamically more favorable. At this point, the film rewets the Pt(111) surface. The increase in CO oxidation activity, which correlates with rewetting, provides strong support for the previously suggested mechanism of CO oxidation on FeO(111)/Pt(111) with the O−Fe−O trilayer as the most active phase.[29]

4. CONCLUSION

In this study, we investigated the reactivity of FeO(111)/Pt(111) toward water and oxygen in the mbar pressure range using both experimental and computational techniques. The FeO(111) film is rather inert toward molecular water with only limited water dissociation even at a water vapor pressure of 10 mbar. In the presence of high molecular oxygen partial pressure (10−100 mbar), the FeO(111) film transforms into a (Pt−)O−Fe−O trilayer that readily reacts with water to form a (Pt−)O−Fe−OH film. The hydroxylated trilayer film was shown to be similarly active in CO oxidation as the nonhydroxylated one. DFT calculations addressing the interaction of water with FeO-(111)/Pt(111) as well as the phase diagram of FeO_xH_y/Pt determined by ab initio thermodynamics are perfectly in line with the experimental results. The hydroxylated film maintains long-range order and is stable in air and even in liquid water environment.

■ ASSOCIATED CONTENT

Supporting Information. XPS and IRAS data obtained for the interaction of H radicals with FeO(111)/Pt(111) and IRAS data for H_2O adsorption on FeO(111)/Pt(111) in UHV at 90 K. This material is available free of charge via the Internet at http://pubs.acs.org.

■ AUTHOR INFORMATION

Corresponding Author

*E-mail: sterrer@fhi-berlin.mpg.de (M.S.); livia.giordano@mater.unimib.it (L.G.).

Author Contributions

#These authors contributed equally to the work.

■ ACKNOWLEDGMENT

Y.F. is grateful to DAAD and Co. Ltd. Takata for a fellowship. H.W. thanks the International Max Planck Research School "Complex Surfaces in Materials Science" for a fellowship. E.C. is grateful to the MICINN of Spain for a fellowship. This work was supported by the Cluster of Excellence "Unifying Concepts in Catalysis" sponsored by the Deutsche Forschungsgemeinschaft (DFG) and administered by TU Berlin. We thank Regione Lombardia and CILEA Consortium through a LISA Initiative (Laboratory for Interdisciplinary Advanced Simulation) for a CPU grant.

■ REFERENCES

(1) Thiel, P. A.; Madey, T. E. *Surf. Sci. Rep.* **1987**, *7*, 211.
(2) Henderson, M. A. *Surf. Sci. Rep.* **2002**, *46*, 1.
(3) Goniakowski, J.; Finocchi, F.; Noguera, C. *Rep. Prog. Phys.* **2008**, *71*, 016501.
(4) Rohr, F.; Wirth, K.; Libuda, J.; Cappus, D.; Bäumer, M.; Freund, H.-J. *Surf. Sci.* **1994**, *315*, L977.
(5) Goniakowski, J.; Giordano, L.; Noguera, C. *Phys. Rev. B* **2010**, *81*, 205404.
(6) Pacchioni, G.; Giordano, L.; Baistrocchi, M. *Phys. Rev. Lett.* **2005**, *94*, 226104.
(7) Sterrer, M.; Risse, T.; Martinez Pozzoni, U.; Giordano, L.; Heyde, M.; Rust, H.-P.; Pacchioni, G.; Freund, H.-J. *Phys. Rev. Lett.* **2007**, *98*, 096107.
(8) Goniakowski, J.; Noguera, C. *Phys. Rev. B* **2009**, *79*, 155433.

(9) Giordano, L.; Pacchioni, G.; Goniakowski, J.; Nilius, N.; Rienks, E. D. L.; Freund, H.-J. *Phys. Rev. Lett.* **2008**, *101*, 026102.
(10) Goniakowski, J.; Noguera, C.; Giordano, L.; Pacchioni, G. *Phys. Rev. B* **2009**, *80*, 125403.
(11) Kim, Y. J.; Westphal, C.; Ynzunza, R. X.; Galloway, H. C.; Salmeron, M.; Van Hove, M. A.; Fadley, C. S. *Phys. Rev. B* **1997**, *55*, 13448.
(12) Weiss, W.; Ranke, W. *Prog. Surf. Sci.* **2002**, *70*, 1.
(13) Rienks, E. D. L.; Nilius, N.; Rust, H.-P.; Freund, H.-J. *Phys. Rev. B* **2005**, *71*, 241404.
(14) Merte, L. R.; Grabow, L. C.; Peng, G.; Knudsen, J.; Zeuthen, H.; Kudernatsch, W.; Porsgaard, S.; Lægsgaard, E.; Mavrikakis, M.; Besenbacher, F. *J. Phys. Chem. C* **2011**, *115*, 2089.
(15) Nilius, N.; Rienks, E. D. L.; Rust, H.-P.; Freund, H.-J. *Phys. Rev. Lett.* **2005**, *95*, 066101.
(16) Rienks, E. D. L.; Nilius, N.; Giordano, L.; Goniakowski, J.; Pacchioni, G.; Felicissimo, M. P.; Risse, T.; Rust, H.-P.; Freund, H.-J. *Phys. Rev. B* **2007**, *75*, 205443.
(17) Giordano, L.; Pacchioni, G.; Goniakowski, J.; Nilius, N.; Rienks, E. D. L.; Freund, H.-J. *Phys. Rev. B* **2007**, *76*, 075416.
(18) Lin, X.; Nilius, N. *J. Phys. Chem. C* **2008**, *112*, 15325.
(19) Berdunov, N.; Mariotto, G.; Balakrishnan, K.; Murphy, S.; Shvets, I. V. *Surf. Sci.* **2006**, *600*, L287.
(20) Knudsen, J.; Merte, L. R.; Grabow, L. C.; Eichhorn, F. M.; Porsgaard, S.; Zeuthen, H.; Vang, R. T.; Lægsgaard, E.; Mavrikakis, M.; Besenbacher, F. *Surf. Sci.* **2010**, *604*, 11.
(21) Xu, L.; Zhang, W.; Zhang, Y.; Wu, Z.; Chen, B.; Jiang, Z.; Ma, Y.; Yang, J.; Huang, W.-X. *J. Phys. Chem. C* **2011**, *115*, 6815.
(22) Huang, W.-X.; Ranke, W. *Surf. Sci.* **2006**, *600*, 793.
(23) Joseph, Y.; Ranke, W.; Weiss, W. *J. Phys. Chem. B* **2000**, *104*, 3224.
(24) Daschbach, J. L.; Dohnálek, Z.; Liu, S.-R.; Smith, R. S.; Kay, B. D. *J. Phys. Chem. B* **2005**, *109*, 10362.
(25) Leist, U.; Ranke, W.; Al-Shamery, K. *Phys. Chem. Chem. Phys.* **2003**, *5*, 2435.
(26) Deng, X.; Lee, J.; Wang, C.; Matranga, C.; Aksoy, F.; Liu, Z. *Langmuir* **2011**, *27*, 2146.
(27) Kim, Y. K.; Zhang, Z.; Parkinson, G. S.; Li, S.-C.; Kay, B. D.; Dohnálek, Z. *J. Phys. Chem. C* **2009**, *113*, 20020.
(28) Sun, Y.-N.; Qin, Z.-H.; Lewandowski, M.; Carrasco, E.; Sterrer, M.; Shaikhutdinov, S.; Freund, H.-J. *J. Catal.* **2009**, *266*, 359.
(29) Sun, Y.-N.; Giordano, L.; Goniaksowski, J.; Lewandowski, M.; Qin, Z.-H.; Noguera, C.; Shaikhutdinov, S.; Pacchioni, G.; Freund, H.-J. *Angew. Chem., Int. Ed.* **2010**, *49*, 4418.
(30) Giordano, L.; Lewandowski, M.; Groot, I. M. N.; Sun, Y.-N.; Goniakowski, J.; Noguera, C.; Shaikhutdinov, S.; Pacchioni, G.; Freund, H.-J. *J. Phys. Chem. C* **2010**, *114*, 21504.
(31) Lewandowski, M.; Sun, Y.-N.; Qin, Z.-H.; Shaikhutdinov, S.; Freund, H.-J. *Appl. Catal., A* **2011**, *391*, 407.
(32) Wilms, M.; Kruft, M.; Bermes, G.; Wandelt, K. *Rev. Sci. Intrum.* **1999**, *70*, 3641.
(33) Dudarev, S. L.; Botton, G. A.; Savrasov, S. Y.; Humphreys, C. J.; Sutton, A. P. *Phys. Rev. B* **1998**, *57*, 1505.
(34) Kresse, G.; Hafner, J. *Phys Rev. B* **1993**, *47*, 558.
(35) Kresse, G.; Furthmüller, J. *Phys. Rev. B* **1996**, *54*, 11169.
(36) Perdew, J. P.; Chevary, J. A.; Vosko, S. H.; Jackson, K. A.; Pederson, M. R.; Singh, D. J.; Fiolhais, C. *Phys. Rev. B* **1992**, *46*, 6671.
(37) Blöchl, P. E. *Phys Rev. B* **1994**, *50*, 17953.
(38) Bengone, O.; Alouani, M.; Blöchl, P. E.; Hugel, J. *Phys Rev. B* **2000**, *62*, 16392.
(39) Reuter, K.; Scheffler, M. *Phys. Rev. B* **2002**, *65*, 035406.
(40) Ritter, M.; Ranke, W.; Weiss, W. *Phys. Rev. B* **1998**, *57*, 7240.
(41) Schedel-Niedrig, T.; Weiss, W.; Schlögl, R. *Phys. Rev. B* **1995**, *52*, 17449.
(42) Brundle, C. R.; Chuang, T. J.; Wandelt, K. *Surf. Sci.* **1977**, *68*, 459.
(43) Muhler, M.; Schlögl, R.; Ertl, G. *J. Catal.* **1992**, *138*, 413.
(44) Russell, J. D.; Parfitt, R. L.; Fraser, A. R.; Farmer, V. C. *Nature* **1974**, *248*, 220.
(45) Shaikhutdinov, S. K.; Meyer, R.; Naschitzki, M.; Bäumer, M.; Freund, H.-J. *Catal. Lett.* **2003**, *86*, 211.
(46) Lemire, C.; Meyer, R.; Shaikhutdinov, S.; Freund, H.-J. *Angew. Chem., Int. Ed.* **2004**, *43*, 118.
(47) Brown, M. A.; Fujimori, Y.; Ringleb, F.; Shao, X.; Stavale, F.; Nilius, N.; Sterrer, M.; Freund, H.-J. *J. Am. Chem. Soc.* **2011**, *133*, 10668.
(48) Matthey, D.; Wang, J. G.; Wendt, S.; Matthiesen, J.; Schaub, R.; Lægsgaard, E.; Hammer, B.; Besenbacher, F. *Science* **2007**, *315*, 1692.
(49) Brown, M. A.; Carrasco, E.; Sterrer, M.; Freund, H.-J. *J. Am. Chem. Soc.* **2010**, *132*, 4064.